International Journal of GEOMATE, June, 2016, Vol. 10, Issue 22, pp. 1964-1970
Geotec., Const. Mat. & Env., ISSN: 2186-2982(Print), 2186-2990(Online), Japan

IMAGE PROCESSING FOR GEOTECHNICAL LABORATORY MEASUREMENTS

Erica Elice Saloma Uy[1] and Tirawat Boonyatee[2]

[1]Civil Engineering, De La Salle University, Philippines; [2] Chulalongkorn University, Thailand

ABSTRACT: This research is an effort to apply image processing techniques for non-contact determination of 2D and 3D displacements of specimens in a triaxial apparatus. For the 2D measurement, a calibration procedure is applied to correct image distortions before the positions of interested points are tracked by the pyramidal optical flow algorithm (Lucas and Kanade, 1981). By considering the change of position, the displacement of an interested point can be determined. The results are compared with the measurements obtained from LVDTs and are well agreed. For 3D measurement, calibration, rectification, correspondence and 3D re-projection are performed. It is verified by an isotropic compression test of a cylindrical sponge in a triaxial apparatus. The estimated displacement and discharge of water are compared with the measured ones and are well agreed. The repeatability and resolution of the developed system are found to be in the order of 0.006 cm and 0.004 cm, respectively.

Keywords: Image Processing, Non-Contact Measurement, Optical Flow, Stereo Vision System

1. INTRODUCTION

Geotechnical measurements have provided the life and blood for advances in modern geotechnical engineering [1]. Since the development of soil mechanics in 1930s, innovations have been made to achieve more precise, accurate and reliable measurements. Over the years, several techniques in measuring the displacement of soil are developed. Techniques such as full-field measurements, which can also be referred to as a non-contact measurement, began to flourish by providing better understanding compared to point-wise measurements. In contrast to conventional sensors such as linear variable differential transducers (LVDTs), deformation can be determined without any direct contact with the target of measurement [2]. Image processing is becoming a trend especially in the field of Geotechnical Engineering in determining measurements. The advent of digital image processing resulted in powerful measuring techniques such as Digital photogrammetry, particle image velocimetry (PIV) and digital image correlation (DIC) [3],[4].

This study is an effort to develop a system that incorporates non-contact measurement through image processing. The system aims to determine the displacement and volume change of soil specimens in a triaxial apparatus. Lucas and Kanade pyramidal optical flow algorithm is applied to track the movement of the soil [5], [6]. Non-contact measurements are made with respect to 2D and 3D axes. Triaxial tests are performed to validate the displacements and volume change the system measured. The advantage of this technique is that on-line and off-line measurement can be done through the pictures taken. Furthermore, monitoring of the progression of failure zones within the sample as it is being tested is possible. In order to integrate this system, Labview is used as the software to develop programs that can implement image processing, optical flow and monitoring.

2. OPTICAL FLOW ALGORITHM

Optical flow can be defined as the changes in gray values that occur within the image plane through successive images [5]. It has the dimensions of velocity were it can be denoted as $\vec{v} = (u, v)$ where u and v are the x and y components of the optical flow vector at a point. When the optical flow is obtained from two successive images, the optical flow vector will appear as a displacement vector $\vec{d} = (d_x, d_y)$ where d_x and d_y are the x and y components of the displacement vector at a point.

An optical flow algorithm has the capability in estimating the changes in motion of a certain point within the image under the assumption that brightness is constant among the subsequent images [7]. Lucas and Kanade pyramidal optical flow algorithm is a type of feature based approach. The method establishes correspondence of feature points between the varying images at a certain time interval. Furthermore, it analyzes two grayscale images, I and J, having $\vec{x} = (x, y)$ as the pixel location within the image plane. Thus, $I(\vec{x}) = I(x, y)$ and $J(\vec{x}) = J(x, y)$. Let image $I(\vec{x})$ be the first image while image $J(\vec{x})$ the second image. When a point of concern, $\vec{s} = (s_x, s_y)$, is established in the first image the algorithm will track its location $\vec{t} = \vec{s} + \vec{d}$ in the second image. $I(\vec{s})$ and $J(\vec{t})$ must be almost equal and have a similar brightness in the two dimensional neighborhood. Equation (1) defines the expression used to track the points and determine the image displacement $\vec{d}$ where it is the vector that minimizes the residual function $\varepsilon(\vec{d})$ [5].

$$\varepsilon(\vec{d}) = \varepsilon(d_x, d_y) = \sum_{x=u_x-\omega_x}^{u_x+\omega_x} \sum_{y=u_y-\omega_y}^{u_y+\omega_y} [I(x,y) - J(x+d_x, y+d_y)]^2 \quad (1)$$

where

ω_x, ω_y = arbitrary numbers that ranges from 1, 2, 3 or more pixels

3. CALIBRATION

3.1 Stage 1: 2D Camera Calibration

Prior to the calibration for the stereo vision system, 2D camera calibration is performed to eliminate the distortion. Two Canon 650D cameras with 18-55 mm f/3.5-5.6 IS II Kit Lens are used and pointed parallel towards the triaxial apparatus. This stage involves the determination of the internal and external parameters of cameras. The focal length, optical center and distortion coefficients are known as the internal parameters. Tangential and radial distortion coefficients are the most common types encountered in calibrating a camera. On the other hand for the external parameters, it is composed of a rotation matrix and translation vector. Presented in this section are procedures for calibrating a single camera which were implemented in Labview.

1.) A panel of dotted grid having a spacing of 2 cm center to center is placed in front of the object of concern. The camera must capture different orientations of the panel in a range of + 20 degrees. Caution must be made to ensure that the first image is in the field of view of the camera so that the dots can be visibly seen.
2.) Threshold is performed to extract the grid feature of the calibration panel from pictures taken from the previous step.
3.) The calibration axis is established at the upper left corner of the grid.
4.) The internal, distortion and external parameters are estimated.

3.2 Stage 2: Calibration for 3D Measurement

In this stage a cube is placed inside the triaxial cell together with water to determine the appropriate focal length, baseline or separation between the two cameras and image resolution. The cube is used since its straight edges can be easily detected by image processing routines. The cube is 9.9x7.5x6 cm. The parameters were varied until they provide a good coverage area of the object of concern. From this test, the cameras must be placed at the back of the apparatus at 113 cm. Cameras are mounted on the wall so that it can have stable support. A focal length of 55 mm and base line of 20 cm is used to have a better view of the object as it is being tested. An image resolution of 1920x1280 pixels is implemented since it can capture the whole object with less distortion.

4. 2D IMAGE PROCESSING

4.1 Accuracy Check

A rubber cylinder with a height of 12.7 cm and a diameter of 5.8 cm is used to check the accuracy of the system. An angle bar is attached on the perimeters of the specimen to serve as the support for the LVDT. Three strain gauges are also attached at the top, middle and bottom part of the specimen. Lucas and Kanade pyramidal optical flow algorithm is used to track the movements of marked points. 10 sets of readings up to a displacement of 1.27 cm are performed in steps of 0.5 mm and 1 mm. From the test, a resolution of 0.2 mm is obtained. Strains are derived from displacements obtained from image processing and compared to the readings from a strain gage. Unfortunately, there is a large discrepancy because of the difference in the size of gage length used. The strain gage measures at a single point over a gage length of 6 mm while the strain is computed over a wider distance.

4.2 Triaxial Test

Two Bangkok soft clay samples taken from depths of 6 to 7 m (BH1) and 9 to 10 m (BH2) were tested. A grid of dots is drawn on the membrane to serve as targets. A ruler is placed inside the triaxial cell to serve as a reference during the test. Consolidated drained compression unloading triaxial test is performed having a cell pressure of 50 kPa for BH1 and 100 kPa for BH2. For the compression unloading part of the test, it is done by increasing the deviator stress while reducing the cell pressure so that the mean effective stress decreased. Pictures are taken every hour with the use of timer remote controls.

The displacements, external and internal, is obtained through image processing and compared to the reading from a LVDT. The external measurement is made by selecting a region of interest at the top most part of the triaxial cell. It can be observed from Fig. 1 and 2 that the results of both measurement techniques are well agreed. For the internal measurement, the whole region within the coverage of the cameras is tracked. Among the entire region tracked, the area close to the pedestal has the best fit as seen in Fig. 3 and 4. From the test, failures occurred at the mid-section. For the region near the top cap, a small movement was observed. These observations can be clearly seen in Fig. 5 and 6.

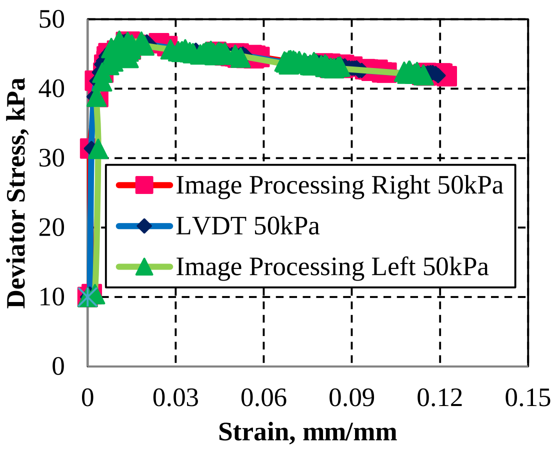

Fig. 1 Stress strain curve for BH1

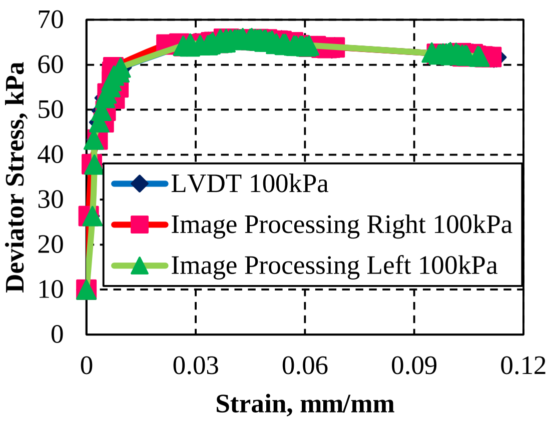

Fig. 2 Stress strain curve for BH2

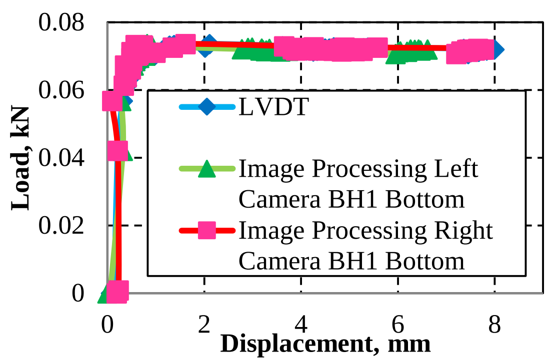

Fig. 3 Load vs displacement curve for BH1

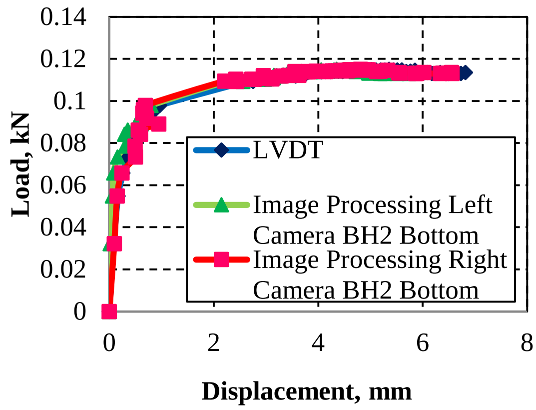

Fig. 4 Load vs displacement curve for BH2

5. COLOR MAPPING

To further monitor the behavior of the soil the displacement and strain field were calculated. A color magnification mapping technique is applied to determine the areas where large deformations occur. This technique is inspired from the research done at Massachusetts Institute of Technology. The pixel values are amplified to reveal hidden information within the image [8]. Their technique can be referred to as Eulerian video magnification. From this, a program is developed in Labview where a color map containing amplified values is plotted and overlaid to the image. This served as an early detection of critical zone of the soil as seen in Fig. 5 and 6. Three base colors in the program are red, green and blue. Red represents a large displacement while blue is for a small displacement. The program developed has a capability of showing only large displacements and strains by making small values transparent. The strain is computed from the change in displacement between two points dividing by the length between them. The grid size used for this computation is 1x1 pixel or 0.26x0.26 mm.

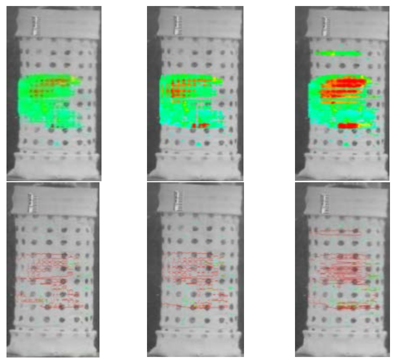

Fig. 5 Color mapping, displacement field (above) and strian field (below), for BH1 from the left camera at day 1, 2 and end of the test.

In Fig. 6, it shows that the sample BH2 tends to have a large movement at the middle in the first few days of the test. This would mean that the soil is undergoing a bulging failure. During the shearing stage, the triaxial cell is being pushed from the bottom. Therefore large displacements can also be expected near the base. Large strain localizations are visible where large displacements occurred. From the color map, non-homogeneous movement is seen as the soil experiences failure.

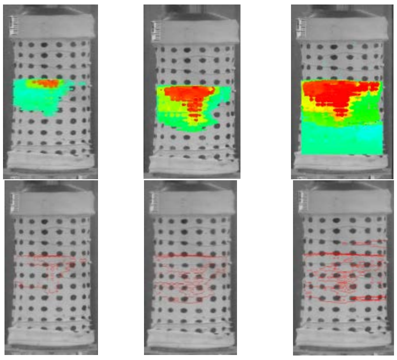

Fig. 6 Color mapping, displacement field (above) and strian field (below), for BH2 from the left camera at day 1, 2 and end of the test.

6. STEREO VISION SYSTEM

Stereo vision system utilizes two cameras to determine the 3D position of a desired point.

6.1 Calibration

For the stereo vision calibration there are two phases. First, the cameras are calibrated independently. The process is similar for calibrating a camera that measures 2D deformation. Second, stereo calibration is performed. This process is defined as the computation of the geometrical relationship between the two cameras [9]. Error statistics, as shown in Table 1, are also obtained to check if the calibration data is valid. The calibration quality and the rectification should be within the range of 0.7 to 1.0. Having a calibration quality of 1.0 would mean that the system is perfectly calibrated. On the other hand the maximum rectification error should not exceed 1.5.

6.2 Rectification

Stereo image rectification is a process when the image planes produced by the left and right camera are being aligned [9]. This process comes right after the stereo calibration since distortion should first be corrected. It helps simplify the stereo correspondence computation. From the error statistics obtained from the stereo calibration, the rectification error should always be satisfied. This maintains the accuracy of the system to perform mapping.

Table 1 Error statistics of stereo calibration

Error Statistics	Result
Max Projection Error	1.99
Calibration Quality	0.83
Max Rectification Error	1.45
Rectification Quality	0.9

6.3 Stereo Correspondence

Stereo correspondence is the stage when the match between the field of view of the left and right image is mapped [10]. A disparity map is obtained during this step. The overlapping view of the two cameras produces an almost equal disparity value thus the disparity image would highlight the objects within that region. To achieve this, the object of concern must be the dominant one in the scene. Furthermore, a uniform light condition is essential to avoid errors such as shadows form other objects in the scene.

Stereo correspondence is performed along the overlapping view through sum of absolute differences (SAD) window. The SAD algorithm is an area-based correspondence algorithm. It computes the intensity differences for each center pixel (i,j) in a window v_x by v_y [11]. To have a better correspondence, a bigger window size is advisable.

6.4 Depth Mapping

The depth map can be obtained through the process called reprojection. It is performed at a particular reference rectified image. For the program's case the left rectified image served as the reference. The reprojection matrix (Q), Eq. (3), is used to reproject the 2D coordinates at the rectified image together with the corresponding disparity value into its 3D position [9].

$$\begin{bmatrix} X \\ Y \\ Z \\ W \end{bmatrix} = Q \cdot \begin{bmatrix} x \\ y \\ d \\ 1 \end{bmatrix} \tag{2}$$

$$Q = \begin{bmatrix} 1 & 0 & 0 & -c_x \\ 0 & 1 & 0 & -c_y \\ 0 & 0 & 0 & f \\ 0 & 0 & -1/T_x & (c_x - c'_x)/T_x \end{bmatrix} \tag{3}$$

where
c_x = horizontal distance from the principal point to the optical center on the image plane of the left image
c_y = vertical distance from the principal point to the optical center on the image plane of the left image
f = focal length
T_x = baseline
c'_x = horizontal distance from the principal point to the optical center on the image plane of the right image
W = weight

6.5 Accuracy Check

6.5.1 Validation for depth reading

To thoroughly check the accuracy of the system, a small card board was attached on a micrometer. It is placed on the triaxial base at a distance of 105 cm from the cameras. Ten readings are made when the cardboard was moved in steps of 0.05, 0.1, 0.2, 0.4, 0.6, and 0.8 cm along the micrometer axis. The standard deviation from both increments are computed and used to express the repeatability of the system. The coefficient of variation of the system is found to be around 0.006381 to 0.078066. The repeatability and accuracy of the system is determined from the standard deviation and it is found to be 0.006 cm and 0.004 cm, respectively.

6.5.2 Validation for depth reading under tilting planes

In order to determine the capacity of the system to read depth changes under tilting planes, a laser transducer was used to get the profile of a deformed sample and it is compared to the result of the system. Oil clay is used as a sample since it is easy to manipulate. Readings are made at the center, 40º from the center and boundary of the sample. The profile is read for 10 times at the center and 40º from the center of the sample. For the profile at the boundary of the sample, only 3 readings are made. The measurements from the stereo vision system and the laser transducer are compared. From the test, errors at the center has a range of 0.39 to 0.90 mm, errors at 40º from the center has a range of 0.64 to 4.62 mm, and errors at the boundary has a range of 0.79 to 1.87 mm. Large errors are observed from the readings at 40º from the center. Stereo correspondence search is difficult to perform at this area since it is at the maximum camera coverage.

6.6 Triaxial Test

Initially tests are planned to be done on Bangkok Clay samples but a sponge is used instead to avoid non-homogeneous mode of deformation. The use of sponge provided a better control on the flow of water. Six trials are made in determining the capacity of the system. The amount of water flowing in and out of the sponge is calculated by three different techniques.

For the first technique, the reference image is taken before the beginning of test. In this manner the cumulative volume of water can be measured. This method only worked for a certain amount of time because it became difficult to estimate movements from significantly different image pair. For the second technique, the reference image is taken right after the cell pressure and back pressure has been applied. The volume obtained from this technique is also a cumulative one. Similarly the algorithm worked over a limited period. In the third technique, the change in volume between successive images is determined. For all methods**,** percentage errors in a range of 1.16 to 8.86% are observed. When the size of patch is varied to examine its influence on the calculated result, no distinct trend was observed. A large amount of water is introduced to the sponge to determine its limitation. Using the second method, the volume of inflow calculated is 43.16 cc while the measured volume is 45.88 cc and error of 6.1% is observed.

The capacity of the system to measure at displacements is also determined. 3 Unconsolidated undrained tests are performed using Bangkok clay. Unfortunately, only 1 trial can be analyzed because the images of the other trials are not in good condition. An error of 1.77 to 10.14% is observed from the measured external displacements. The internal displacements on the other hand are measured at the midsection of the soil sample since it is the critical area. Fluctuations are encountered when the displacements and strains are computed. To further investigate on this, displacements at the pedestal, 1/3 from the base and 2/3 from the base was obtained and compared with the result from the LVDT. From Fig. 7, it can be seen that fluctuations started at a deviator stress greater than 15 kPa at 2/3 from the base. To have a better understanding on what occurred during the test full-field monitoring was performed. Displacement fields are shown in Fig. 7 and it can be seen that there are localizations at the area 2/3 from the base. Due to this, it is impossible to measure the internal displacements for this data.

7. CONCLUSION

A non-contact measurement system was developed and it had the capacities to perform 2D and 3D measurements through image processing. Lukas and Kanade pyramidal optical flow algorithm is applied in both measurements to track the movement of interested points.

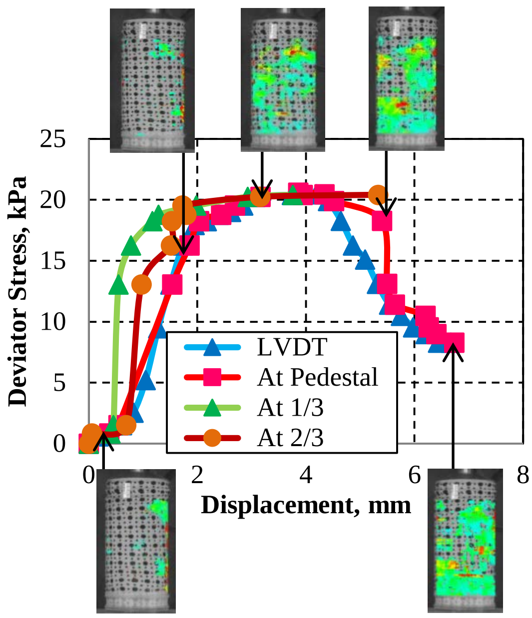

Fig. 7 Stress-displacement plot for Bangkok Clay

The 2D measuring system's resolution is found to be 0.2 mm. When the readings from the system are compared to those from LVDT, for a consolidated drained unloading test errors ranging from 5 to 10% are observed. For the 3D measuring system, when an unconsolidated undrained test is performed errors ranging from 1.77 to 10.14% are observed. When measuring out of plane movements, the repeatability and resolution is found to be 0.006 cm and 0.004 cm, respectively. For the readings of depth at titling planes the profile from the system is compared with a laser transducer. Large differences can be observed at 40º from the center at a range of 0.64 to 4.62 mm. Errors ranging from 1.16 to 8.86% are obtained when computed volumes are compared with measured values. The system provides an option to compute the volume of flow between any image pair. From these, it can be concluded that the system has a good capability in obtaining 2D and 3D measurements. It can be applied in monitoring the behavior of the soil during the test such as to monitor the development of localization failures in soil. However, it is only limited to the area viewable by the cameras.

8. ACKNOWLEDGEMENTS

I would like to thank AUN/SEED-Net and JICA for their generosity in funding this research and giving me the opportunity to pursue graduate studies. Furthermore, I would like to thank and express my greatest gratitude to my family, friends and mentors who always gave me the unconditional support that I need in going through this journey. I am forever grateful to my adviser who helped me broaden my knowledge and skills in my field of specialization. More so, I am thankful to my seniors and juniors who helped me in developing my research. Lastly, I would like to thank God for giving me the courage, wisdom and humility to pursue higher studies.

9. REFERENCES

[1] Marr WA, "Advances and Retreats in Geotechnical Measurements", Judgment and Innovation: The Heritage and Future of the Geotechnical Engineering Profession, 2000, pp. 42-60.

[2] Viggiani, G. amd Hall, SA, "Full-field Measurements, A New Tool for Laboratory Experimental Geomechanics", Paper presented at the Proceedings of the 4th International Symposium on Deformation Characteristics of Geomaterials (Burns SE, Mayne PW and Santamarina JC (Eds.)), 2008, pp.3-26.

[3] Xing, ZX, Wells, LG, Yaping, J and Shearer, SA, "Using Image Analysis to Measure Two-Dimensional Soil Deformation", Journal of Terramechanics, Vol 34, 1997, pp. 73-82.

[4] Khosravi, M, Tang, L, Pipatpongsa, T, Takemura, J, and Doncommul, P, "Performance of Counterweight Balance in Stability of Undercut Slope Evaluated by Physical Modeling", International Journal of Geotechnical Engineering, Vol 6, 2012, pp. 193-20.

[5] Fernando, WSP, Udawatta, L, and Pathirana, P, "Identification of Moving Obstacles with Pyramidal Lucas and Kanade Optical Flow and K Means Clustering", Proceedings on the 2007 Third International Conference on Information and Automation for Sustainability, 2007, pp. 111-117.

[6] Lucas, BD and Kanade, T, "An Iterative Image Registration Technique with an Application to Stereo Vision", Proceedings of Imaging Understanding Workshop, 1981, pp. 121-130.

[7] Mahalingam, V, Bhattacharya, K, Ranganathan, N, Chakravarthula, H, Murphy, RR and Pratt, KS "A VLSI Architecture and Algorithm for Lucas-Kanade Based Optical Flow Computation", IEEE Transaction on Very Large Scale Integration (VLSI) Systems, 2010, pp. 29-38.

[8] Wu, HY, Rubinstein, M, Shih, E, Guttag, J, Durand, F, and Freeman, WT, "Eulerian Video Magnification for Revealing Subtle Changes in the World", ACM Transactions on Graphics, Volume 31, 2012.

[9] Bradski, G and Kaehler, A, "Projection and 3D Vision", Learning OpenCV Computer Vision with the OpenCV Library, O'Reilly, 2008, pp.405-458.

[10] Saidon, MS, Desa, H, Murugesa, P and Rosbi, MSM "Developing Stereo Vision System for Object Recognition and Positioning of AMAD-R Mobile Robot", Proceedings of the International Conference on Man-Machine Systems, 2009, pp. 3B8-1-5.

[11] Kuhl, K. "Comparison of Stereo Matching Algorithms for Mobile Robots", The University of Western Australia, Australia, 2005

International Journal of GEOMATE, June, 2016, Vol. 10, Issue 22, pp. 1964-1970.

MS No. 5175 received on June 15, 2015 and reviewed under GEOMATE publication policies.

Pertinent discussion including authors' closure, if any, will be published in Feb. 2017 if the discussion is received by Aug. 2016.

Corresponding Author: Erica Elice Saloma Uy